Prediction of fatigue life with interspersed mode-I and mixed-mode (I and II) overloads by an exponential model: Extensions and improvements

J.R. Mohanty, B.B. Verma and P.K. Ray

http://dx.doi.org/10.1016/j.engfracmech.2008.12.001

Engineering Fracture Mechanics
Volume 76, Issue 3, February 2009, Pages 454-468

Prediction of fatigue life with interspersed mode-I and mixed-mode (I and II) overloads by an exponential model: Extensions and improvements

J.R. Mohanty [a], B.B. Verma [a], P.K. Ray [b,*]

[a] Department of Metallurgical and Materials Engineering, National Institute of Technology, Rourkela 769 008, India
[b] Department of Mechanical Engineering, National Institute of Technology, Rourkela 769 008, India

A B S T R A C T

The current work is an extension of the authors' earlier work and presents a life prediction methodology under interspersed mode-I and mixed-mode (I and II) overloads. The important controlling parameter in the model is 'specific growth rate' (m). It depends on two crack driving forces i.e. stress intensity factor range and maximum stress intensity factor as well as material parameters i.e. fracture toughness, Young's modulus, and yield stress. The dependence of 'm' on these parameters is correlated through a dimensionless parameter 'l'. It is observed that the present model predicts the end life of post-overload period well in case of 7020 T7 and 2024 T3 Al-alloys.

1. Introduction

Despite advances made in the field of engineering design and testing, failure due to fatigue is a common phenomenon and estimation of fatigue life of a component is still in the developing stage. All structures contain flaws either from metallurgical defects or from the damage induced during service. These flaws or cracks grow from an initial size to a critical size leading to catastrophic failure of the structures when subjected to fatigue loading. Design of modern sophisticated equipment against fatigue demands both safety and economy. Hence, there is the need for an accurate life prediction methodology so that a component may be replaced before a catastrophic failure occurs.

Although Paris [1] law is the most widely used crack growth law, the first work is attributed to A K Head, an Australian Defence Science and Technology Organization (DSTO) researcher [2]. Later, using Head's observations, Frost and Dugdale [3,4] reported that fatigue crack could grow exponentially leading to a simple log–linear relationship given by:

$$Ln(a) = \varpi N + Ln(a_0) \quad \text{or} \quad a = a_0 e^{\varpi N} \tag{1}$$

which can be written as:

$$\frac{da}{dN} = \varpi a \tag{2}$$

where N is the fatigue life, ϖ is a parameter that depends on the geometry, material and load scenario, a is the crack length and a_0 is the initial flaw size. For constant amplitude loading they found that ϖ could be expressed as:

$$\varpi = f(\sigma) = \psi(\Delta\sigma)^3 \tag{3}$$

* Corresponding author. Tel.: +91 661 2462518.
E-mail addresses: pkray@nitrkl.ac.in, prabal_kray@yahoo.com (P.K. Ray).

Nomenclature

a	crack length (mm) measured from the edge of the plate
a_0	initial crack length (mm)
a_i	crack length corresponding to the 'ith' step (mm)
a_i	crack length corresponding to the 'jth' step (mm)
a_f	final crack length (mm)
a_{th}	an intrinsic crack length related to the threshold stress intensity factor
a^{ol}	crack length at overload (mm)
a^*	constant in the generalized Frost and Dugdale law
a_d	retarded crack length (mm)
a_d^P	retarded (predicted) crack length (mm)
a_d^E	retarded (experimental) crack length (mm)
A', B', C', D'	curve fitting constants in the Exponential Model
B	plate thickness (mm)
COD	crack opening displacement
$C_1, \tilde{C}$	fatigue crack growth constants in the generalized Frost and Dugdale law
da/dN	crack growth rate (mm/cycle)
E	modulus of elasticity (MPa)
$f(g)$	geometrical factor
F	remotely applied load (N)
ΔF	remotely applied load range (N)
F_{max}	maximum load of constant amplitude load cycle (N)
F_{min}	minimum load of constant amplitude load cycle (N)
K	stress intensity factor (MPa$\sqrt{m}$)
K_I	mode-I stress intensity factor (MPa$\sqrt{m}$)
K_{II}	mode-II stress intensity factor (MPa$\sqrt{m}$)
K_C	plane stress fracture toughness (MPa$\sqrt{m}$)
$(K_I)_C$	plane stress fracture toughness in mode-I (MPa$\sqrt{m}$)
$(K_{II})_C$	plane stress fracture toughness in mode-II (MPa$\sqrt{m}$)
K_{IIC}	plane strain fracture toughness (MPa$\sqrt{m}$)
K_{max}	maximum stress intensity factor (MPa$\sqrt{m}$)
$K_{max,appl}$	maximum applied stress intensity factor (MPa$\sqrt{m}$)
$K_{max,tot}$	total maximum applied stress intensity factor (MPa$\sqrt{m}$)
K_{max}^B	maximum (base line) stress intensity factor (MPa$\sqrt{m}$)
K_{eq}^{ol}	equivalent stress intensity factor at overload (MPa$\sqrt{m}$)
K_I^{ol}	mode-I stress intensity factor at overload (MPa$\sqrt{m}$)
K_{II}^{ol}	mode-II stress intensity factor at overload (MPa$\sqrt{m}$)
ΔK	stress intensity factor range (MPa$\sqrt{m}$)
ΔK_{eq}	equivalent stress intensity factor (crack driving force) in Frost and Dugdale law (MPa$\sqrt{m}$)
ΔK^+	tensile part of the stress intensity factor range (MPa$\sqrt{m}$)
$\frac{K_{II}}{K_I+K_{II}}$	mode-mixity
l	dimensionless factor in the 'Exponential Model' formulation
m	specific growth rate
m_{ij}	specific growth rate corresponding to the interval i–j
N	number of cycles or fatigue life
N_i	number of cycles corresponding to the 'ith' step
N_j	number of cycles corresponding to the 'jth' step
N_f	final number of cycles
N_d	number of delay cycles
N_d^P	number of delay cycles (predicted)
N_d^E	number of delay cycles (experimental)
N_f^P	final number of cycles (predicted)
N_f^E	final number of cycles (experimental)
q	driving force constant
R^{ol}	overload ratio
t	time

w	plate width (mm)
ϖ	exponent in the Frost and Dugdale crack growth law
$X_1 \ldots X_4, Y_1 \ldots Y_4$ and $Z_1 \ldots Z_4$	curve fitting constants in the 'Exponential Model'
ν	Poisson's ratio
α_1	ratio of mode-I and mode-II plane stress fracture toughness
β	loading angle
β_{IC}	fracture toughness correlation factor
η	generalized Frost and Dugdale fatigue crack growth equation exponent
Ψ	constant in the Frost and Dugdale law
φ	fatigue crack growth equation exponent
σ_{ys}	yield point stress (MPa)
σ_{ut}	ultimate stress (MPa)

where ψ is a constant. Several researchers also observed this exponential nature of growth [5–10] of fatigue cracks by conducting a wide range of full-scale fatigue tests and coupon tests under service spectra. Barter et al. [11] verified the applicability of Eq. (1) for various materials and specimen configurations loaded by both constant amplitude and complex variable amplitude spectra. The relationship between crack growth rate and crack length (Eq. (2)) not only holds good for metallic materials but also for composite repairs as observed by Jones et al. [12].

This observation of crack growth led to the formulation of the generalized form of Frost and Dugdale law [13–15]:

$$\frac{da}{dN} = C_1 (a/a^*)^{(1-\eta/2)} (\Delta K_{eq})^{\eta} = \tilde{C} a^{(1-\eta/2)} (\Delta K_{eq})^{\eta} \tag{4}$$

where ΔK_{eq} is the crack driving force, C_1, a^* and η are constants, and $\tilde{C} = C_1 / a^{*(1-\eta/2)}$.

Further, according to two parameter crack driving force model, also known as Unified Approach [16–21], the crack growth law takes the form:

$$\frac{da}{dN} = C \left[(\Delta K^{+})^{(1-q)} K_{max,appl}^{q} \right]^{\phi} \tag{5}$$

where ΔK^{+} corresponds to the tensile part of the load cycle, q is the driving force constant and φ is the fatigue crack growth equation exponent. Later Jones et al. [22] linked the generalized Frost and Dugdale law (Eq. (4)) to the two parameter fatigue crack growth model (Eq. (5)) and formulated a new functional form of the crack growth rate law:

$$\frac{da}{dN} = (a/a_{th})^{1-\phi/2} C_1 \left(\Delta K_{tot}^{(1-q)} (K_{max,tot}) \right)^{\phi} = (a)^{1-\phi/2} \tilde{C} \left(\Delta K_{tot}^{(1-q)} (K_{max,tot})^{q} \right)^{\phi} \tag{6}$$

where $\tilde{C} = C_1 / a_{th}^{1-\phi/2}$. They used the above formulation to predict the crack growth for a simple laboratory test on D16 Al-alloy specimens as well as for two full scale air-craft fatigue tests (F111 and FIA-18).

In real situations, a structure or a component may be subjected to mixed-mode overload due to either change in the loading direction during service or the presence of randomly oriented defects. Several researchers [23,24] have conducted fatigue tests to study the effect of mixed-mode (I and II) overloads on subsequent mode-I fatigue crack growth. But from life prediction point of view, no model is available, to the knowledge of the authors, so far as mixed-mode overloads are concerned. The Exponential Model, proposed earlier by the authors [25] to evaluate the various retardation parameters, supports the principle of conventional Frost and Dugdale's crack growth law [3,4] as well as the law (Eq. (6)) formulated by Jones et al. [22]. However, the exponent 'm' (specific growth rate) in the proposed exponential model has been treated in a different manner supporting the 'Unified Approach' principle. In the present investigation, the authors have tentatively extended the previously proposed 'Exponential Model' for prediction of fatigue life under interspersed mode-I and mixed-mode (I and II) overload. The model has been tested on both 7020 T7 and 2024 T3 Al-alloys and covers both the regimes-II and -III of fatigue crack growth rate curve.

2. Model development

2.1. Description of the previous exponential model [25]

Prediction of fatigue life in case of mixed-mode overload is more complex than that of mode-I overload because of the involvement of different angles of overloading. As a first step, an attempt was made to predict the a–N curve of post-overload portion up to the end of retardation. This was done using different overload ratios (R^{ol} = 2.5, 2.6, 2.7 and 2.8) on 7020 T7 Al alloy specimens.

The crack growth equation was written in the following form:

$$a = a_0 e^{mN} \tag{7}$$

$$\text{Or,} \quad m = \frac{\ln\left(\frac{a}{a_0}\right)}{N} \tag{8}$$

where a is crack length in general, a_0 is the initial crack length, N is the number of cycles and m is the specific growth rate.

The specific growth rate m was correlated with a parameter 'l' to take into account the various crack driving parameters such as K_{max}, ΔK, and K_{eq}^{ol} as well as the material properties E and σ_{ys} by a linear curve-fit for the retardation portion of the post-overload period as described below:

$$m = A'l + B' \tag{9}$$

where

$$l = \left[\frac{K_{eq}^{ol}}{K_{max}}\right] \times \left[\frac{K_{eq}^{ol}}{\Delta K}\right] \times \left[\frac{E}{\sigma_{ys}}\right] \tag{10}$$

Since the constants A' and B' were different for different angles of overload, they were again correlated with mode mixity $\frac{K_{II}}{K_I+K_{II}}$ by polynomial curve fitting. By putting the values of the above constants in Eq. (8), the predicted values of m were calculated for the loading angle 54° corresponding to respective crack lengths. The predicted number of cycles (fatigue life) was calculated as follows:

$$N = \frac{\ln\left(\frac{a}{a_0}\right)}{m} \tag{11}$$

2.2. Proposed modifications – an extension of the earlier model

(1) Although the Exponential Model of the form $a = a_0 e^{mN}$ can be effectively used to determine the retardation parameters a_d and N_d, the major inconsistency arises while calculating the specific growth rate m. It is known that fatigue life is sensitive to initial crack length [26]. However, calculation of m in the region a_0–a_f will only give an average value of m in that region as observed in the earlier model. As the value of m changes with each increment of crack length, it will be more appropriate to calculate specific growth rate, m, at each crack length increments considering the present crack length as the initial one for the successive step. Eqs. (7), (8) are, therefore, modified in the following forms:

$$a_j = a_i e^{m_{ij}(N_j - N_i)} \tag{12}$$

$$\text{Or,} \quad m_{ij} = \frac{\ln\left(\frac{a_j}{a_i}\right)}{(N_j - N_i)} \tag{13}$$

where a_i and a_j are crack lengths in ith step and jth step in 'mm', respectively, N_i and N_j number of cycles in ith step and jth step, respectively, m_{ij} is the specific growth rate in the interval i–j, i is the number of experimental steps and $j = i + 1$.

(2) The power term in the exponential equation is a dimensionless quantity and hence l should be dimensionless. As such the terms $\left(\frac{K_{eq}^{ol}}{\Delta K}\right)$, $\left(\frac{K_{eq}^{ol}}{K_{max}}\right)$ and $\left(\frac{E}{\sigma_{ys}}\right)$ in the expression of 'l' are acceptable from the dimensional analysis point of view. However, it will be more appropriate if ΔK, K_{max}, and σ_{ys} are used in the numerators as these parameters control the growth rate directly though this may not give a straight line fit between m and l.

(3) A single tensile overload retards the crack growth rate, whether the overload is in mode-I or mixed-mode, and hence increases the residual life. In the earlier reported work [25], modeling was done for the post-overload period to calculate only the retardation parameters. Since the ultimate aim is to estimate the residual life of the component, K_{eq}^{ol}

Table 1
Curve-fitting constants of 7020 T7 alloy.

Overload angle (β)	Mode-mixity $\left(\frac{K_{II}}{K_I+K_{II}}\right)$	$A' \times 10^{-6}$	$B' \times 10^{-6}$	$C' \times 10^{-6}$	$D' \times 10^{-6}$
90°	1	−539649	145310	−10994.00	259.79
72°	0.755	−502381	134367	−9829.70	220.57
54°	0.579	−409896	107374	−7065.30	130.42
36°	0.421	−398478	104031	−6853.30	126.11
18°	0.245	−375919	98609	−6562.20	122.74
0°	0	−352141	91313	−5839.90	97.56

Table 2
Curve fitting constants of 2024 T3 alloy.

Overload angle (β)	Mode-mixity $\left(\frac{K_{II}}{K_I+K_{II}}\right)$	$A' \times 10^{-6}$	$B' \times 10^{-6}$	$C' \times 10^{-6}$	$D' \times 10^{-6}$
90°	1	−317743	130554	−14954.0	526.86
72°	0.755	−161221	66285	−7576.1	270.48
54°	0.579	−138722	55634	−5523.5	153.62
36°	0.421	−123760	49826	−5091.6	148.40
18°	0.245	−131140	53025	−5560.5	170.22
0°	0	−184424	75502	−8449.2	284.73

in the 'l' parameter is replaced by K_C (to take care of regime-III of the fatigue crack growth curve) and the modified equation is written as:

$$l = \left[\left(\frac{\Delta K}{K_C}\right)\left(\frac{K_{max}}{K_C}\right)\left(\frac{\sigma_{ys}}{E}\right)\right]^{1/4} \tag{14}$$

Table 3
Chemical composition of the two alloys.

Mats.	Al	Cu	Mg	Mn	Fe	Si	Zn	Cr	Others
7020 T7	Main constituent	0.05	1.2	0.43	0.37	0.22	4.6	–	–
2024 T3	90.7–94.7	3.8–4.9	1.2–1.8	0.3–0.9	0.5	0.5	0.25	0.1	0.15

Table 4
Mechanical properties of the two alloys.

Material	Tensile strength (σ_{ut}) MPa	Yield strength (σ_{ys}) MPa	Young's modulus (E) MPa	Poisson's ratio (ν)	Plane strain fracture toughness (K_{IC}) MPa$\sqrt{m}$	Plane stress fracture toughness (K_C) MPa$\sqrt{m}$	Elongation
7020 T7	352.14	314.7	70,000	0.33	50.12	236.8	21.54% in 40 mm
2024 T3	469	324	73,100	0.33	37.0	95.31	19% in 12.7 mm

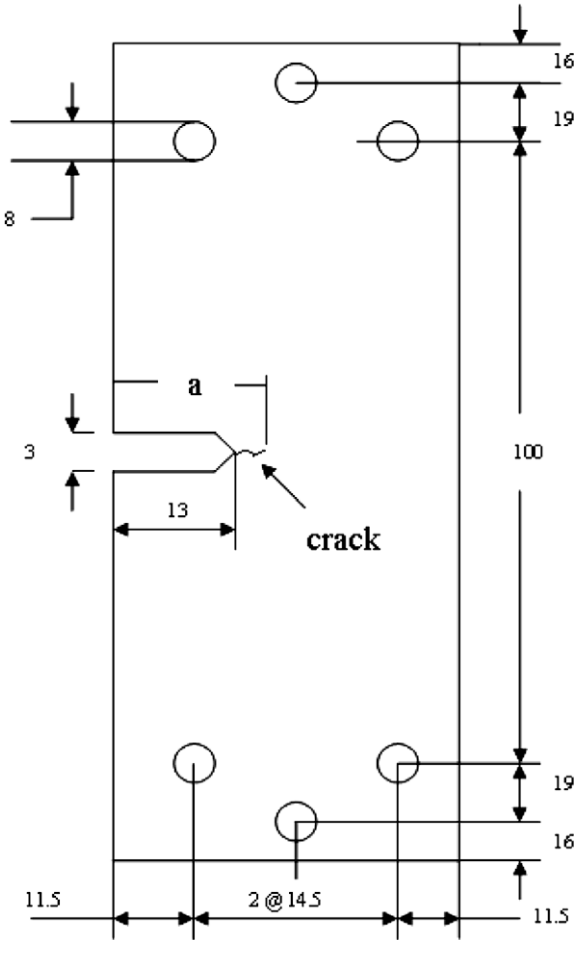

Fig. 1. Single Edge Notch Tension (SENT) Specimen geometry.

Table 5
Load scenarios of the test on two materials.

Material	F_{max} (KN)	F_{min} (KN)	R^{ol}	a_i (mm)	a^{ol} (mm)	a_f (mm)
7020 T7	8.429	0.843	2.5	17.75	19.10	31.2
2024 T3	7.197	0.720	2.5	17.75	20.40	32.40

2.3. Procedural steps for the extended model

In this work single overload with overloading ratio R^{ol} = 2.5 is considered for all loading angles (0°, 18°, 36°, 54°, 72° and 90°) tested on aluminum alloys 7020 T7 and 2024 T3 specimens. The procedural steps of the extended model are as follows:

(1) The value of specific growth rate, *m*, for each step, is calculated from experimental *a*–*N* data using Eq. (13) and subsequently refined by a polynomial curve fit with the calculated '*m*' and '*a*' values.
(2) The refined '*m*' values obtained from step 1 are correlated with the parameter '*l*' to take into account the two crack driving parameters ΔK and K_{max} as per 'unified approach' [16–21] as well as material parameters 'K_C', '*E*', and 'σ_{ys}' represented by the following equation

$$l = \left[\left(\frac{\Delta K}{K_C}\right)\left(\frac{K_{max}}{K_C}\right)\left(\frac{\sigma_{ys}}{E}\right)\right]^{\frac{1}{4}} \tag{15}$$

The values of plane stress fracture toughness (K_C) are calculated from plane strain fracture toughness values (K_{IC}) by an empirical relation proposed by Irwin [27] as presented in following equation

$$K_C^2 = K_{IC}^2(1 + 1.4\beta_{IC}^2) \tag{16}$$

where

$$\beta_{IC} = \frac{1}{B}\left(\frac{K_{IC}}{\sigma_{ys}}\right)^2 \tag{17}$$

The different '*m*' and '*l*' values are fitted by a 3rd degree polynomial for both the materials separately as given below:

$$m = A'l^3 + B'l^2 + C'l + D' \tag{18}$$

where A', B', C' and D' are curve fitting constants. All the values of above constants are listed in Tables 1 and 2, respectively. The values of above constants differ since the amount of retardation varies with the angles of overloading. Therefore, each constant of different overload angles (except 54° angle) are correlated with mode mixity, $\frac{K_{II}}{K_I+K_{II}}$ by a 2nd degree polynomial curve fit so as to give the following sets of equations:

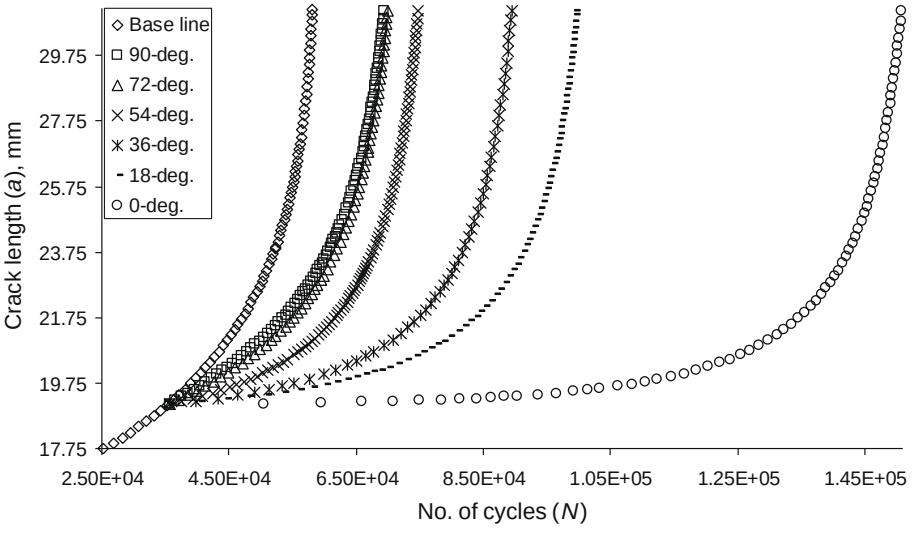

Fig. 2. Comparison of *a*–*N* curves for different overload angles (7020 T7 alloy).

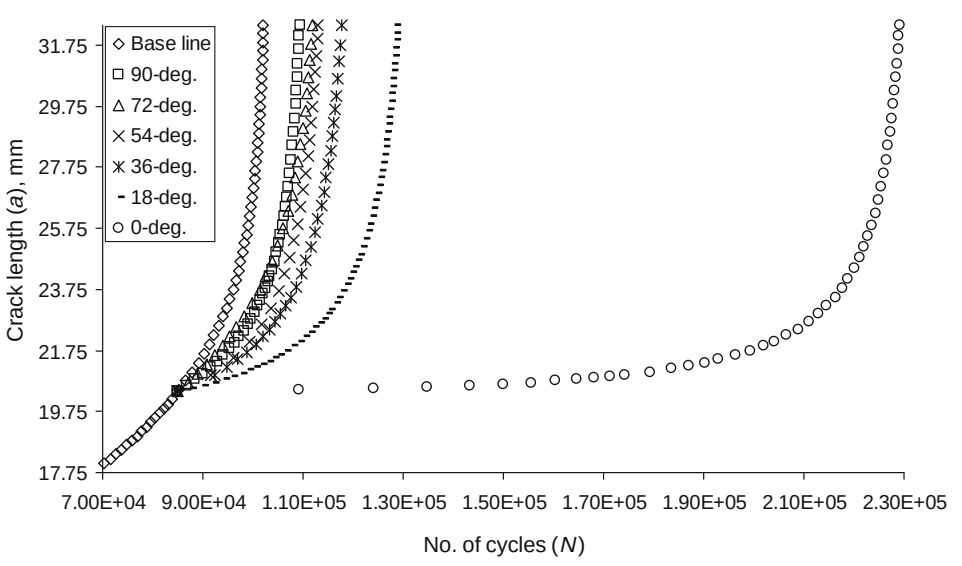

Fig. 3. Comparison of a–N curves for different overload angles (2024 T3 alloy).

$$A' = X_1\left[\frac{K_{II}}{K_I + K_{II}}\right]^2 + Y_1\left[\frac{K_{II}}{K_I + K_{II}}\right] + Z_1 \tag{19}$$

$$B' = X_2\left[\frac{K_{II}}{K_I + K_{II}}\right]^2 + Y_2\left[\frac{K_{II}}{K_I + K_{II}}\right] + Z_2 \tag{20}$$

$$C' = X_3\left[\frac{K_{II}}{K_I + K_{II}}\right]^2 + Y_3\left[\frac{K_{II}}{K_I + K_{II}}\right] + Z_3 \tag{21}$$

$$D' = X_4\left[\frac{K_{II}}{K_I + K_{II}}\right]^2 + Y_4\left[\frac{K_{II}}{K_I + K_{II}}\right] + Z_4 \tag{22}$$

where X_1, X_2, X_3, X_4, Y_1, Y_2, Y_3, Y_4 are another set of curve fitting constants relating A', B', C' and D' with mode mixity $(\frac{K_{II}}{K_I+K_{II}})$. The generalized equation for specific growth rate (Eq. (18)) now becomes:

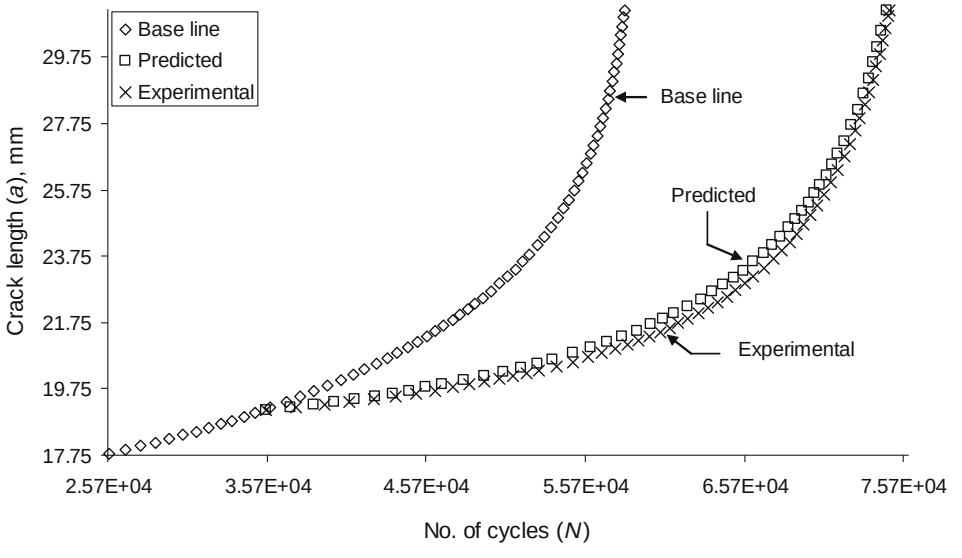

Fig. 4. Comparison of predicted and experimental a–N curves for overload angle 54° (7020 T7 alloy).

$$m = \left\{ X_1 \left[\frac{K_{II}}{K_I + K_{II}} \right]^2 + Y_1 \left[\frac{K_{II}}{K_I + K_{II}} \right] + Z_1 \right\} l^3 + \left\{ X_2 \left[\frac{K_{II}}{K_I + K_{II}} \right]^2 + Y_2 \left[\frac{K_{II}}{K_I + K_{II}} \right] + Z_2 \right\} l^2 + \left\{ X_3 \left[\frac{K_{II}}{K_I + K_{II}} \right]^2 + Y_3 \left[\frac{K_{II}}{K_I + K_{II}} \right] + Z_3 \right\} l + \left\{ X_4 \left[\frac{K_{II}}{K_I + K_{II}} \right]^2 + Y_4 \left[\frac{K_{II}}{K_I + K_{II}} \right] + Z_4 \right\} \quad (23)$$

3. The predicted number of cycle is calculated using the equation:

$$N_j = \frac{\ln\left(\frac{a_j}{a_i}\right)}{m_{ij}} + N_i \quad (24)$$

3. Taking the values of crack lengths and predicted number of cycles, the predicted a–N curves are plotted (overload angle 54°) for both the materials.
4. The crack growth rates, da/dN, are determined directly from the predicted a–N curves obtained above.

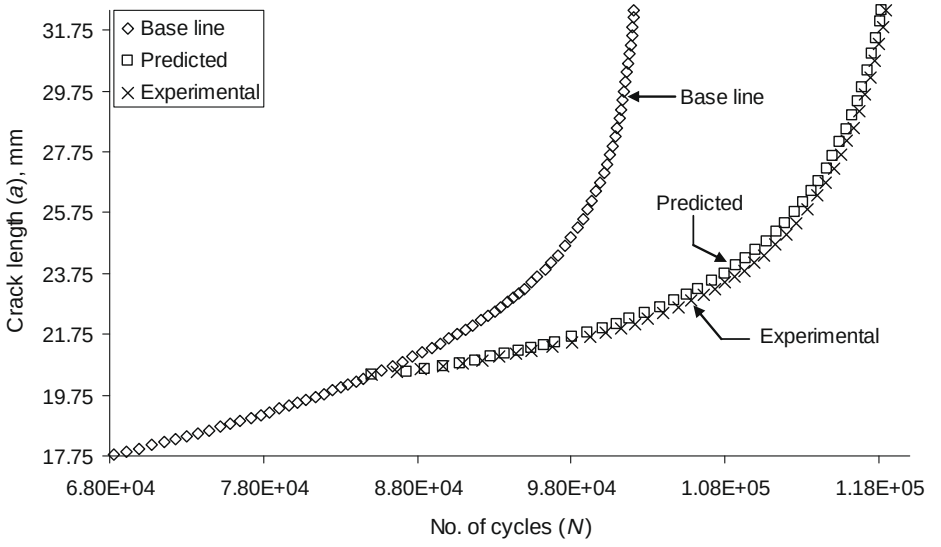

Fig. 5. Comparison of predicted and experimental a–N curves for overload angle 54° (2024 T3 alloy).

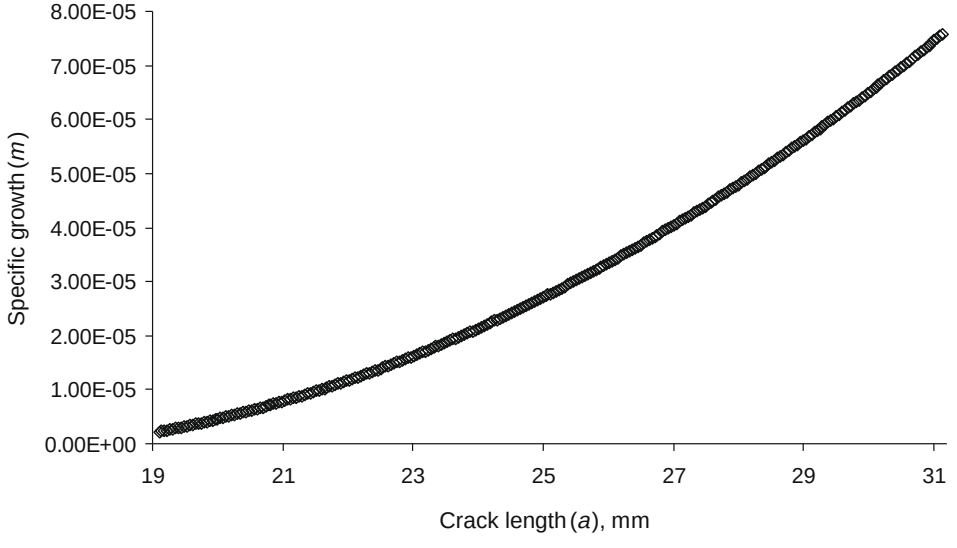

Fig. 6. Variation of specific growth rate (m) with crack length (a) for overload angle 54° (7020 T7 alloy).

5. The values of the stress intensity factor range, ΔK [28] are calculated from the following equation:

$$\Delta K = \mathrm{f}(g)\frac{\Delta F\sqrt{\pi a}}{wB} \tag{25}$$

where

$$\mathrm{f}(g) = 1.12 - 0.231(a/w) + 10.55(a/w)^2 - 21.72(a/w)^3 + 30.39(a/w)^4 \tag{26}$$

3. Experimental procedure

The present investigation was performed on two aluminum alloys (7020 and 2024). The 7020 Al-alloy suitable for ground transport system was procured from Hindalco, Renukoot, India in the as-fabricated condition, while 2024 Al-alloy was procured from Virat Aluminum, Mumbai, India in T3 heat-treated condition. The 7020 Al-alloy was subjected to T7 heat-treatment to obtain optimum mechanical properties. The chemical composition and the mechanical properties of the alloys are given in Tables 3 and 4 respectively.

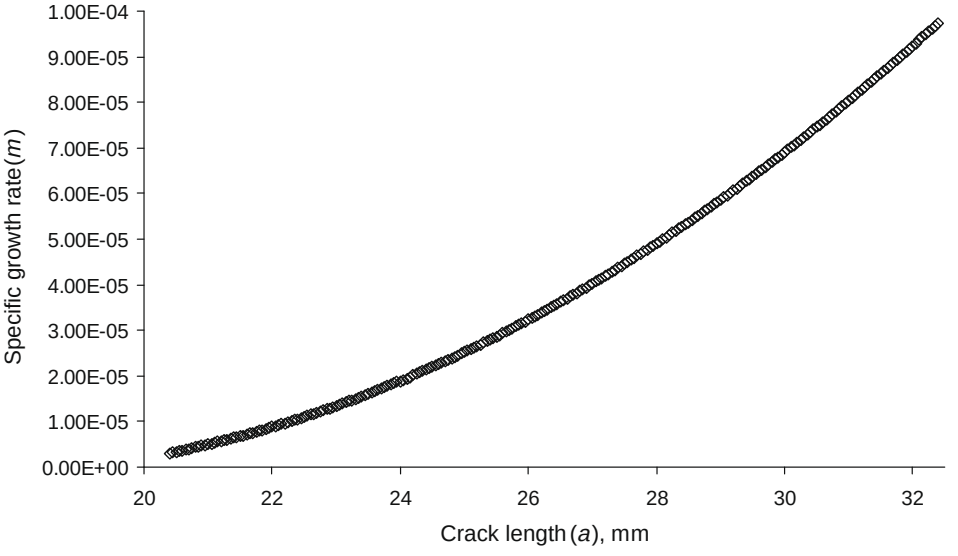

Fig. 7. Variation of specific growth rate (m) with crack length (a) for overload angle 54° (2024 T3 alloy).

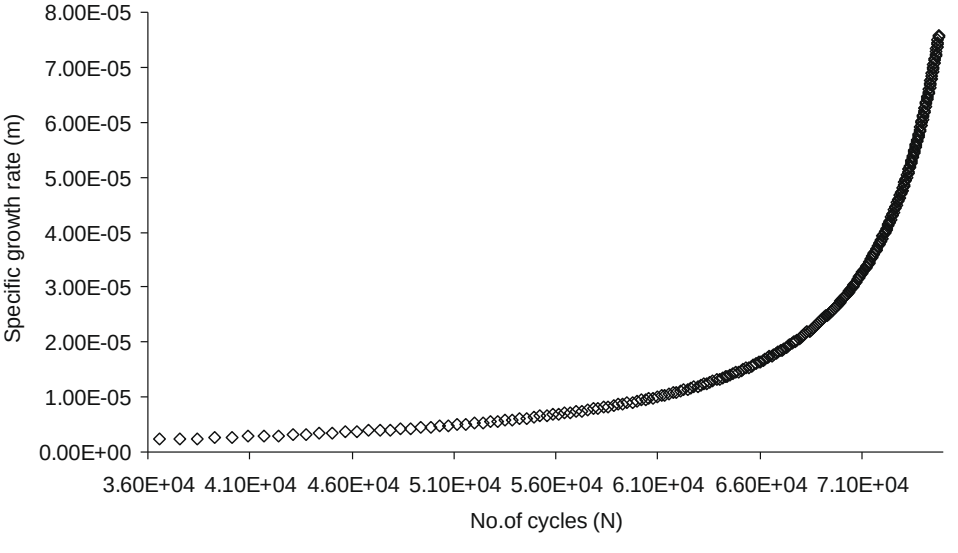

Fig. 8. Variation of specific growth rate (m) with number of cycles (N) for overload angle 54° (7020 T7 alloy).

All the fatigue crack growth tests were conducted in air at room temperature using single-edge notch, SEN specimens made in the longitudinal transverse (LT) direction from the plate. The detail geometry of the specimens is given in Fig. 1. The experiments were performed on a servo-hydraulic *Instron*-8502 machine having a load capacity of 250 kN, interfaced to a computer for machine control and data acquisition. The test specimens were fatigue pre-cracked under mode-I loading to an a/w ratio of 0.3 and were subjected to constant load test (i.e. progressive increase in ΔK with crack extension) maintaining a load ratio of 0.1. The sinusoidal loads were applied at a frequency of 6 Hz. The crack growth was monitored with the help of a COD gauge mounted on the face of the machined notch. The fatigue crack was allowed to grow up to an a/w ratio of 0.4 and subsequently subjected to single overload spike at a loading rate of 8 kN/min. The different load scenarios of both the materials are presented in Table 5.

The overloading was done by using a mixed-mode loading device similar to the one used by Richard [29] and described in the authors' earlier work [25]. The following equations are used to determine stress intensity factors K_I and K_{II} for different angles of overload application

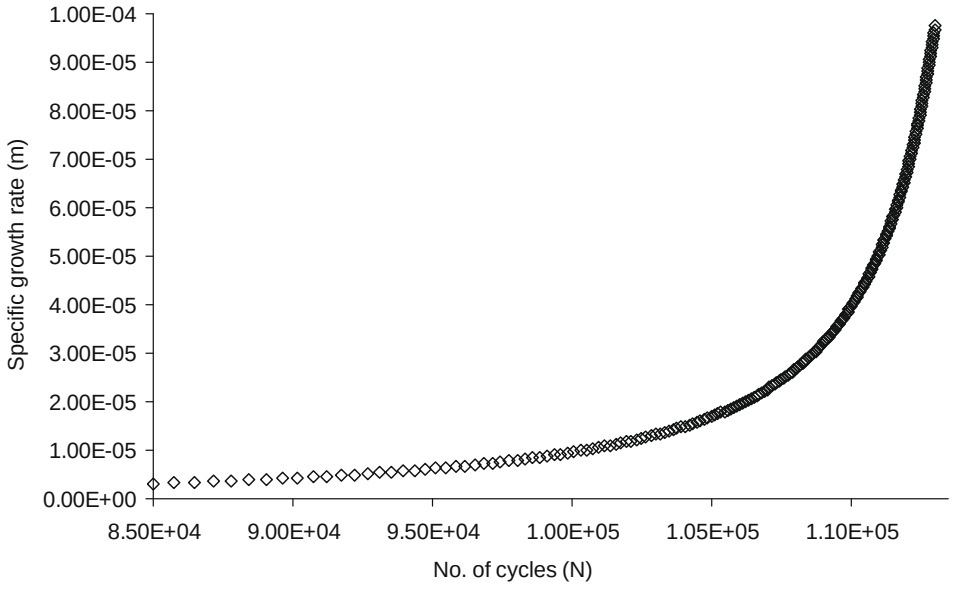

Fig. 9. Variation of specific growth rate (N) with number of cycles (N) for overload angle 54° (2024 T3 alloy).

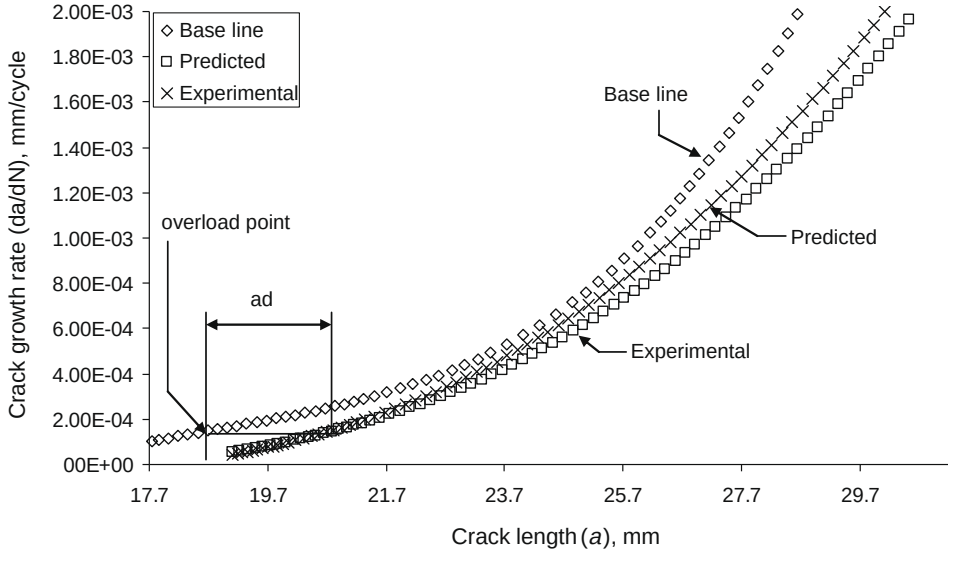

Fig. 10. Comparison of predicted and experimentally obtained retarded crack length (a_d) for overload angle 54° (7020 T7 alloy).

$$K_{\mathrm{I}} = \mathrm{f}(g)\frac{F\cos\beta\sqrt{\pi a}}{wB} \tag{27}$$

$$K_{\mathrm{II}} = \mathrm{f}(g)\frac{F\sin\beta\sqrt{\pi a}}{wB} \tag{28}$$

where f(g) is given in Eq. (26).

The specimens were subjected to mode I, mode II, and mixed-mode overloads at different loading angles, β (= 18°, 36°, 54° and 72°) at an overloading ratio of 2.5. Overloading ratio is defined as

$$R^{\mathrm{ol}} = \frac{K_{\mathrm{eq}}^{\mathrm{ol}}}{K_{\max}^{B}} \tag{29}$$

where $K_{\max}^{B}$ is the maximum stress intensity factor for base line test. The equivalent stress intensity factors ($K_{\mathrm{eq}}^{\mathrm{ol}}$) are calculated according to the following equation [23]:

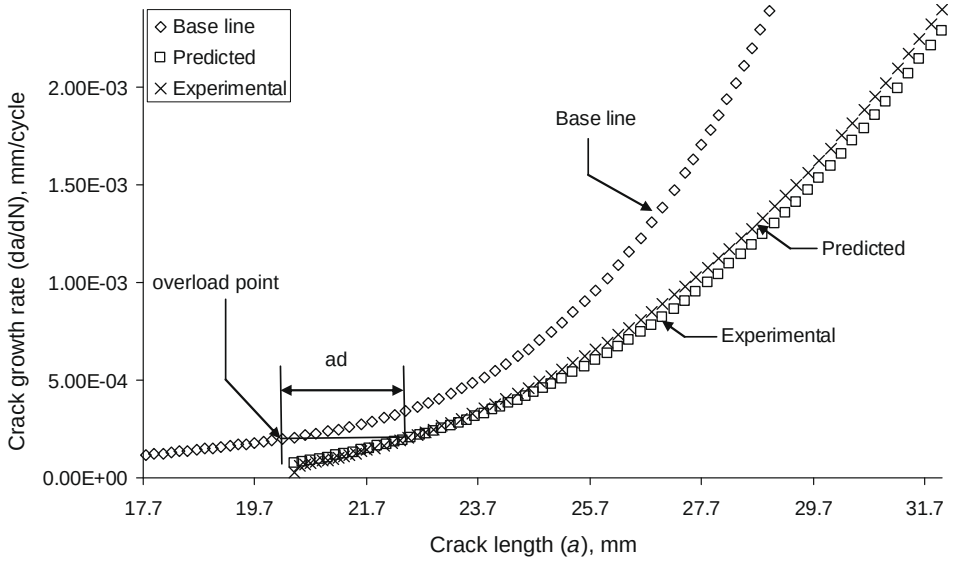

Fig. 11. Comparison of predicted and experimentally obtained retarded crack length (a_{d}) for overload angle 54° (2024 T3 alloy).

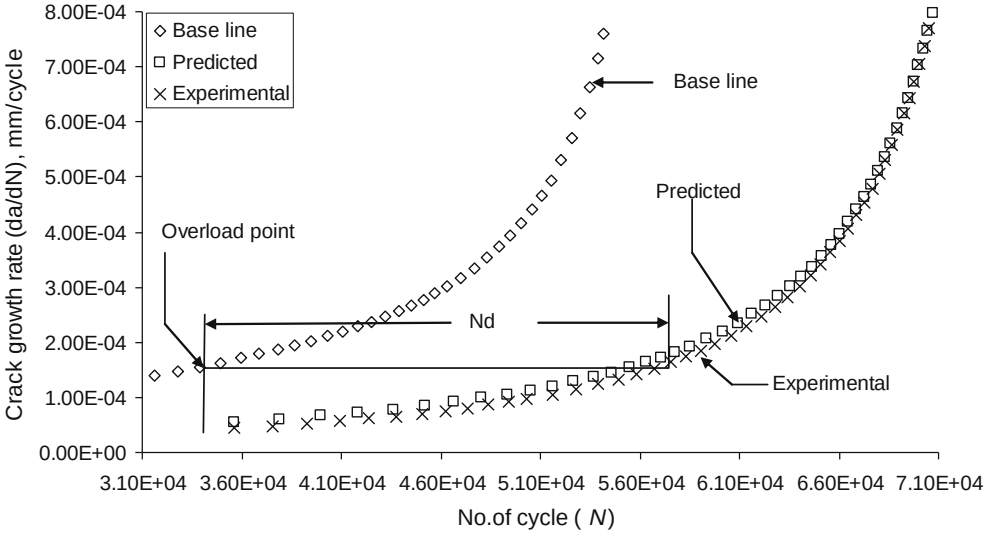

Fig. 12. Comparison of predicted and experimentally obtained delay cycle (N_{d}) for overload angle 54° (7020 T7 alloy).

$$K_{eq}^{ol} = 0.5K_I^{ol} + 0.5\sqrt{(K_I^{ol})^2 + 4(\alpha_1 K_{II}^{ol})^2} \quad (30)$$

where $\alpha_1 = (K_{IC}/K_{IIC}) = 0.95$ according to strain energy density theory [30] and K_I^{ol} and K_{II}^{ol} are the of stress intensity factors of modes I and II during the overload respectively. Then the fatigue test was continued in mode I.

4. Validation of the model with experimental results and discussion

4.1. Model validation

It has been verified by Sander and Richard [23] that a pure Mode-I overload ($\beta = 0°$) leads to maximum retardation, while Mode-II overload ($\beta = 90°$) has least effect on retardation. In the intermediate ranges ($\beta = 18°$, 36°, 54°, and 72°), the single tensile overload has mixed effect (Figs. 2 and 3) due to the presence of shear stress component. The proposed modified mod-

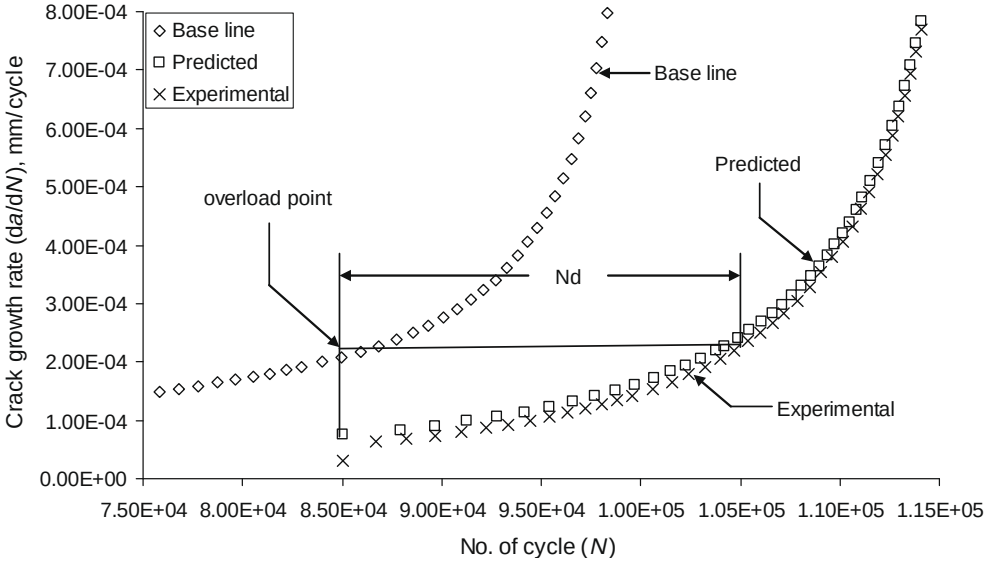

Fig. 13. Comparison of predicted and experimentally obtained delay cycle (N_d) for overload angle 54° (2024 T3 alloy).

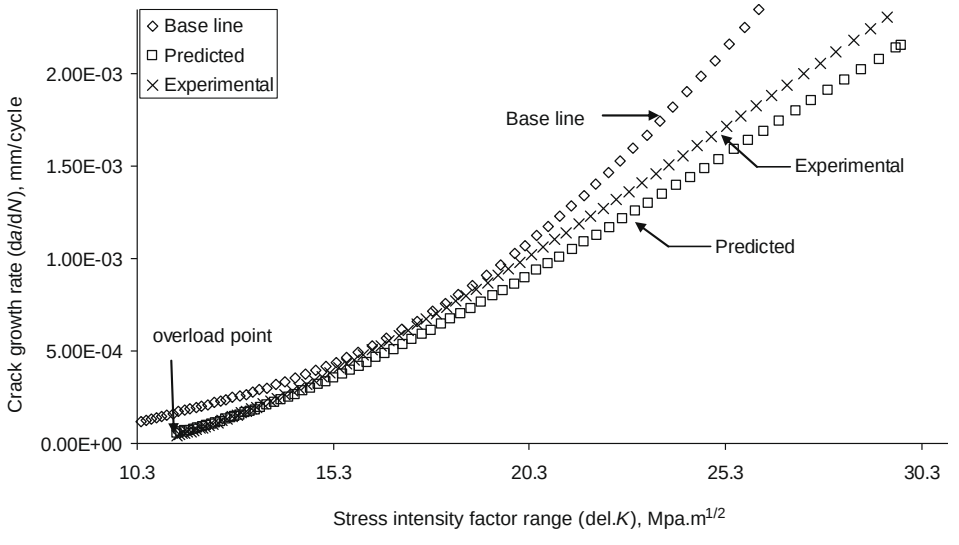

Fig. 14. Comparison of predicted and experimental crack growth rate (da/dN) with stress intensity range (ΔK) for overload angle 54° (7020 T7 alloy).

el has been tested for overload angle of 54° for both materials and the predicted results are compared with the experimental data (Figs. 4–15). Figs. 4 and 5 show the experimental and predicted a–N curves for overload angle 54° and Figs. 6–9 show the variation of specific growth rate (m) with crack length (a) and number of cycles (N) for both alloys. The predicted results and percent deviations of retarded crack length (a_d) and delay cycle (N_d) from experimental values are presented in Table 6 and illustrated in Figs. 10–13 respectively for both materials. The deviations of predicted a_d values for 7020 T7 and 2024 T3 alloys are −0.802% and −1.13%, respectively. Similarly the deviations of predicted N_d values are −1.195% and −2.273%, respectively. The deviations of predicted number of cycles $\left(N_f^p\right)$ from experimental results are −0.238% and −0.217% for 7020 T7 and 2024 T3 alloys, respectively. Figs. 14 and 15 compare the crack growth rate (da/dN) with the stress intensity factor range (ΔK).

4.2. Discussion

The experimental test results in fatigue are noisy and random in nature, although repeated trends can be observed. A good prediction of the fatigue crack growth behavior can be obtained by a stochastic rather than a deterministic differential equation model [31,32]. However, the very purpose of a scientific model is that it must be simple and fast to apply with some physical meaning during its solution process. In conventional differential equation model of Paris [1] there is a physical inconsistency when the constants of the crack growth rate equation are randomized as per dimensional analysis point of view [33]. In the differential equation of the proposed Exponential Model, this type of inconsistency does not arise as the specific growth rate 'm' is a dimensionless parameter. Further, the modified form of the extended Exponential Model minimizes the randomness of the fatigue test data, thereby making the model simpler and faster to apply by increasing its prediction capability.

Spagnoli [34] analyzed the Paris law on the basis of both similarity methods and fractal concepts and presented some experimental evidence of its breakdown of similitude concept. He observed that the complete self-similarity (corresponding to no crack-size dependence of da/dN-ΔK relationship) of Paris law is only possible for larger crack size. Whenever the crack size is small (for micron-sized crack and also in case of concrete or other heterogeneous materials), the crack growth rate depends on crack size leading to incomplete self-similarity (non-self similarity) of Paris law. Based on these facts, he proposed a crack-size dependent Paris law by strengthening the phenomenon of incomplete self-similarity in the fatigue crack growth process. The differential equation of the Exponential Model follows the form proposed by Spagnoli [34] for non-self similar growth and for the growth of a fractal crack emphasizing the fact that crack growth rate is crack size dependent as per Frost and Dugdale law [3,4].

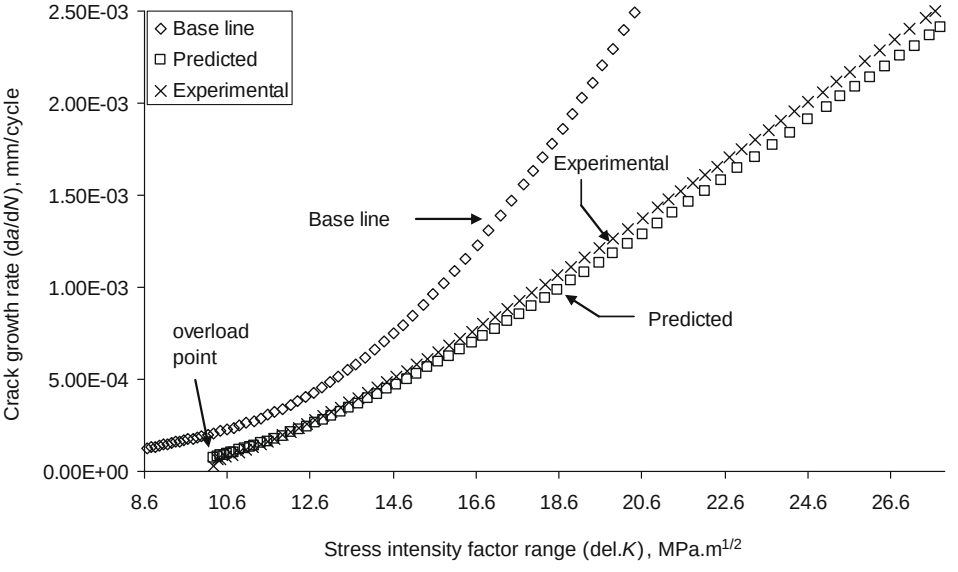

Fig. 15. Comparison of predicted and experimental crack growth rate (da/dN) with stress intensity range (ΔK) for overload angle 54° (2024 T3 alloy).

Table 6
Experimental results of the tested specimens.

Material	a_d^p mm	a_d^E mm	% error in a_d^p	N_d^p Kcycle	N_d^E Kcycle	% error in N_d^p	N_f^p Kcycle	N_f^E Kcycle	% error in N_f^p
7020 T7	1.978	1.994	−0.802	21.49	21.750	−1.195	74.600	74.778	−0.238
2024 T3	2.274	2.300	−1.13	19.564	20.019	−2.273	118.218	118.475	−0.217

Furthermore, most of the fatigue crack growth models are in the form of differential equations relating crack growth rate and stress intensity factor raised to a power of approximately 3. Hence, any inaccuracy in the value of stress intensity factor is magnified in life calculation. The discrepancies may be even more dramatic for initial cracks loaded near the fatigue threshold limit. The involvement of robust numerical integration scheme also makes the life calculation more complicated particularly for variable amplitude loading [35]. But, in the proposed Exponential Model any inaccuracy in the values of crack driving forces does not significantly alter the fatigue life as the specific growth rate '*m*' is related to different crack driving forces raised to a power (highest) of 0.75. However, the only demerit in the model is the determination of various curve fitting constants which requires much effort.

5. Conclusion

(1) 'Extended Exponential Model' of the form $a_j = a_i e^{m_{ij}(N_j - N_i)}$ can be effectively used to determine the retardation parameters a_d and N_d as well as the fatigue life N_f for specimens subjected to mixed-mode (I and II) overload.

(2) The intrinsic growth rate m is a function of two crack driving forces, ΔK, K_{max}, mode mixity $\frac{K_{II}}{K_I+K_{II}}$ and material parameters, E, σ_{ys}, K_C, and can be represented by an equation of the form $m = A'l^3 + B'l^2 + C'l + D'$ where $l = \left[\left(\frac{\Delta K}{K_C}\right)\left(\frac{K_{max}}{K_C}\right)\left(\frac{\sigma_{ys}}{E}\right)\right]^{\frac{1}{4}}$ and A', B', C' and D' are functions of $\frac{K_{II}}{K_I+K_{II}}$.

(3) The differential form of the proposed model conforms the dimensional analysis concept and indicates a dependence of 'da/dN' on 'a' and hence, an existence of incomplete self-similarity in the fatigue crack growth rate phenomenon.

(4) The percentage deviations of retardation parameters, (a_d and N_d) and fatigue life (N_f) predicted by the above model from the experimental data for 7020 T7 and 2024 T3 Al-alloys are found to be within reasonable accuracy.

Acknowledgement

The authors wish to record their thanks to CSIR, India for sponsoring this project (project No. 22(373)/04/EMR II). They also thank Hindalco, Renukoot, India for providing the 7020 Aluminium alloy for this research project.

References

[1] Paris PC, Gomez MP, Anderson WP. A rational analytic theory of fatigue. Trend Engng 1961;13:9–14.
[2] Head AK. The growth of fatigue cracks. Phil Mag 1953;44(7):925–38.
[3] Frost NE, Marsh KJ, Pook LP. Metal fatigue. Oxford: Clarendon Press; 1974.
[4] Frost NE, Dugdale DS. The propagation of fatigue cracks in test specimens. J Mech Phys Solids 1958;6:92–110.
[5] Murakamia Y, Miller KJ. What is fatigue damage? A view point from the observation of low cycle fatigue process. Int J Fatigue 2005;27(8):991–1005.
[6] Polak J, Zezulka P. Short crack growth and fatigue life in austenitic–ferritic duplex stainless steel. Fatigue Fract Engng Mater Struct 2005;28:923–35.
[7] Nisitani H, Goto M, Kawagoishi N. A small-crack growth law and its related phenomena. Engng Fract Mech 1992;41(4):499–513.
[8] Kawagoishi N, Chen Q, Nisitani H. Significance of the small crack growth law and its practical application. Metall Mater Trans 2000;31A:2005–13.
[9] Caton MJ, Jones JW, Boileau JM, Allison JE. The effect of solidification rate on the growth of small fatigue cracks in a cast319-type aluminium alloy. Metall Mater Trans 1999;30A:3055–68.
[10] Goldsmith NT. Fractographic examinations relevant to the F&W Mirage fatigue test. ARL-Mat-Tech-Memo371, Melbourne, Australia; 1978.
[11] Barter S, Molent L, Goldsmith N, Jones R. An experimental evaluation of fatigue crack growth. Engng Fail Anal 2005;12:99–128.
[12] Jones R, Krishnapillai K, Pitt S. Crack patching: predicting fatigue crack growth. Theor Appl Fract Mech 2006;45:79–91.
[13] Pell RA, Molent L, Green AJ. The fractographical comparison of F/A-18 aluminium alloy 7050-T7451 bulkhead representative coupons tested under two fatigue load spectra at several stress levels. DSTO-TR-1547, Melbourne, Australia; February 2004.
[14] Goldsmith N. Fractographic examination of cracking in hole No. 2 of Mirage Wing A3094. DSTO, Letter N86/79NTG 1981; February 1981.
[15] Barter SA. Fatigue crack growth in 7050T7451 aluminium alloy thick section plate with a surface condition simulating some regions of F/A-18 structure. Defence Science and Technology Organisation, DSTO-TR-1458, Melbourne, Australia; July 2003.
[16] Noroozi AH, Glinka G, Lambert S. A two parameter driving force for fatigue crack growth analysis. Int J Fatigue 2005;27:1277–96.
[17] Dinda S, Kujawski D. Corelation and prediction of fatigue crack growth for different R-ratios using K_{max} and ΔK^+ parameters. Eng Fract Mech 2004;71(12):1779–90.
[18] Donald K, Paris PC. An evaluation of ΔK_{eff} estimation procedures on 6060-T6 and 2024-T3 aluminum alloys. Int J fatigue 1999;21:S47–57.
[19] Sadananda K, Vasudevan AK, Holtz RL, Lee EU. Analysis of overload effects and related phenomenon. Int J Fatigue 1999;21:S233–46.
[20] Kujawski D. A new $(\Delta K^+ K_{max})^{0.5}$driving force parameter for crack growth in aluminum alloys. Int J Fatigue 2001;23(8):733–40.
[21] Kujawski D. A fatigue crack driving force parameter with load ratio effects. Int J Fatigue 2001;23:S239–46.
[22] Jones R, Molent L, Pitt S. Crack growth of physically small cracks. Int J fatigue 2007;29:1658–67.
[23] Sander M, Richard HA. Experimental and numerical investigations on the influence of the loading direction on the fatigue crack growth. Int J Fatigue 2006;28:583–91.
[24] Srinivas V, Vasudevan P. Studies of mixed-mode crack propagation in D16AT Al-alloy. Engng Fract Mech 1993;45(4):415–30.
[25] Mohanty JR, Verma BB, Ray PK. Evaluation of overload-induced fatigue crack growth retardation parameters using an exponential model. Engng Fract Mech 2008;75:3941–51.
[26] Hertzberg RW. Deformation and fracture mechanics of engineering materials. 4th ed. New York: John Wiley & Sons, Inc; 1996.
[27] Irwin GR. NRL Report 6598; November 21, 1967.
[28] Brown WF, Srawley JE. Plane strain crack toughness testing of high strength metallic materials. ASTM STP 410. Philadelphia: American Society for Testing and Materials; 1966. p. 1.
[29] Richard HA. Fracture mechanical predictions for cracks with superimposed normal and shear loading. Dusseldorf: VDI-Verlag; 1985 [in German] (in 10).
[30] Suresh S. Fatigue of materials. 1st ed. Cambridge University Press; 1992. p. 351.
[31] Virkler DA, Hillberry BM, Goel PK. The statistical modeling nature of fatigue crack propagation. J Engng Mater Technol ASME 1979;101:148–53.

[32] Ghonem H, Dore S. Experimental study of the constant probability crack growth curves under constant amplitude loading. Engnng Fract Mech 1987;27:1–25.
[33] Maymon G. The problematic nature of the application of stochastic crack growth models in engineering design. Engng Fract Mech 1996;53(6):911–6.
[34] Spagnoli A. Self-similarity and fractals in the Paris range of fatigue crack growth. Mech Mater 2005;37:519–29.
[35] Timbrell C, Chandwani R, Cook G. State of The Art in Crack Propagation. Zentech International Limited, <http://www.zentech.co.uk>; 2004.